Tellus (2003), 55A, 401–418
Printed in UK. All rights reserved

TELLUS
ISSN 0280–6495

Boundary and initial flow induced variability over Pacific North America in CCC-AGCM simulations

By AMIR SHABBAR*, KAZ HIGUCHI and JIANPING HUANG, *Meteorological Service of Canada, Environment Canada, 4905 Dufferin Street, Toronto, Ontario, Canada M3H 5T4*

(Manuscript received 9 September 2002; in final form 10 April 2003)

ABSTRACT

Specified time-varying sea-surface temperatures (SST) of the extreme phases of El Niño-Southern Oscillation (ENSO), sea ice extent and different initial atmospheric flow configurations over the midlatitudes are used in a series of general circulation model (GCM) experiments to analyze variability over the Pacific North American (PNA) sector. These experiments are performed with the second-generation Canadian Climate Centre atmospheric general circulation model, CCC-GCM2 (hereafter referred to as AGCM2). Two-way analysis of variance (ANOVA) and Empirical Orthogonal Function (EOF) techniques are applied to the model results to assess and quantify the effects of the prescribed sea-surface temperatures and different initial flow regimes (zonal and meridional) on the modes of midlatitude variability over the PNA sector. Results show that the prescribed ENSO sea surface temperatures significantly influence the midlatitude simulated variability at 500 hPa in a form of the PNA teleconnection pattern. In addition, the initial flow configuration is seen to have a small but significant effect on midlatitude variability. The interaction between the ENSO effect and the initial flow configuration does not significantly influence the midlatitude atmospheric variability. This indicates the effects of the perturbation of the ENSO SST and the internal atmospheric dynamics on the total variability are additive. The contribution to the total variability over the PNA sector by the specification of the initial atmospheric flow regime also manifests itself in a PNA-like pattern.

1. Introduction

The North Atlantic Oscillation (NAO) and the Pacific North American (PNA) teleconnection pattern are the two most prominent modes of low-frequency variability in the extratropical atmosphere in winter, appearing as mode 1 and mode 2, respectively, in principle-component analysis of Northern Hemisphere height or pressure anomaly fields (Barnston and Livezey, 1987). In particular, it is now generally accepted that the atmospheric circulation variability over the PNA sector in wintertime is significantly influenced by the anomalous sea surface temperature (SST) occurrences associated with El Niño (warm SST anomaly) and La Niña (cold SST anomaly) events in the tropical Pacific Ocean (Mo et al., 1998). This atmosphere–ocean coupling is referred to as ENSO (El Niño-Southern Oscillation), and includes both the cold and warm SST anomaly forcings in the tropical Pacific. Typically, the dynamical forcing of the tropical Pacific SST anomaly appears as a standing Rossby wave in the troposphere, with energy propagating from the tropics to the midlatitudes, characteristically producing a pattern reminiscent of the PNA teleconnection pattern over North America (Hoskins and Karoly, 1981; Opsteegh and Van den Dool, 1980). As a result, ENSO events in the eastern tropical Pacific induce significant temperature and precipitation anomalies over the North American continent (Ropelewski and Halpert, 1986; Shabbar and Khandekar, 1996).

Hoerling and Kumar (1997) suggest that there are two main contributing causes to the ENSO variability over the North American continent: (1) midlatitude atmospheric sensitivity to the tropical Pacific SST forcing in magnitude and spatial extent, and/or

*Corresponding author.
e-mail: amir.shabbar@ec.gc.ca

(2) the atmospheric state that results due to the internal non-linear dynamical interactions of the atmosphere, as well as to non-SST boundary forcings (such as snow cover). The ENSO SST forcing on the midlatitude flow variability has already been examined in some detail by a number of investigators; however, the relative contribution of the latter cause needs to be further explored. Among these non-ENSO related processes for generating and maintaining the PNA pattern of variability might be instability of zonally varying climatological mean flow (Simmons et al., 1983) and midlatitude transient eddies associated with storm tracks (Kok and Opsteegh, 1985). Additionally, Geisler et al. (1985) have suggested that on the interannual timescale, teleconnections may result from the excitation of barotropically unstable modes. The North Pacific sector is particularly favoured for the genesis of such modes, since it lies in the exit region of the Asian jet, and during times of anomalous SSTs extraction of energy from the mean flow may give rise to such modes.

SSTs are the dominant source of interannual variability in the tropics, and their impact on the midlatitude circulation is well known (e.g. Wallace and Gutzler, 1981; Horel and Wallace, 1981). Although the internal chaotic nature of the midlatitudes may obscure the boundary forcing, large boundary-forced effects would still be expected in the midlatitudes. It may be reasonable to ask whether the choice of initial flow configuration in the midlatitudes contributes significantly to the total variability. This variation may arise due to the natural variation of the climate system.

The effects of the initial flow conditions on the atmospheric flow have been previously examined in the Atmospheric Model Intercomparison Project (AMIP; see Gates, 1992) simulations by Zwiers (1996). Results showed no significant additional variability that could be attributed to the initial conditions. However, this could likely be due to the design of the experiment, in which both the nature of the initial conditions and length of the integration were different from those proposed in the present study.

The primary objective of this study is to analyze and quantify the relative contribution of the initial flow configurations prior to the boreal winter season on the variability over the PNA sector. Motivation for focusing on this particular atmospheric process derives from the finding that the atmospheric response in the midlatitudes to the tropical Pacific SSTs is dependent on the midlatitude SST anomaly (Lee et al., 2002) which in turn affects the midlatitude circulation anomalies (Namias et al., 1988; Peng et al., 1997). It is conceivable that the tropical Pacific SST-induced Rossby wave train will interact with the atmospheric circulation to produce different flow patterns in the midlatitudes. Based on the concept that multiple stable flow regimes can exist in the atmosphere for a given set of boundary conditions (Lorenz, 1984), one can speculate on the possibility that, depending on the initial configuration of the midlatitude circulation pattern just prior to the ENSO winter season, a Rossby wave forcing could "slot" the atmosphere into a relatively stable mode of circulation, thus producing some variations in the circulation response over the PNA sector.

There is evidence to suggest that the general circulation climate model used in this study does possess a property of multiple stable flow regimes (Fyfe et al., 1999). If this is true, then the variability in winter climate regime over North America could, at least in part, be attributable to the different initial atmospheric flow patterns. To test this idea, the second generation of the Canadian Climate Centre general circulation model AGCM2 is used to conduct several numerical experiments in which all simulations differ only in their specification of the initial midlatitude atmospheric conditions (zonal vs. meridional flow) over the PNA sector. The domain of the PNA sector is defined as the area bounded by 180° and 40°W and between 20°N and 90°N. The boundary conditions are assumed to be deterministic, since each simulation is forced by the same winter evolution of either El Niño or La Niña SST boundary conditions. The sea ice boundary is made to vary according to the Global Ice and Sea Surface Temperature (GISST) climatology (Parker et al., 1995) and is the same in each model simulation.

The contribution of the boundary-forced and initial-flow configurations towards the total variability over the PNA sector is quantified. Furthermore, it is demonstrated that the two effects are independent of each other.

This study is organized as follows. The experimental design using AGCM2 is described in section 2. Details about the Analysis of Variance (ANOVA) methodology are shown in section 3, followed by results of the model simulations in section 4. The paper closes with a summary and discussion in section 5.

2. Experimental design

AGCM2 provides the basic tool to study the sensitivity of the atmospheric response to the initial

Table 1. *Two factor ANOVA for seasonal and monthly means of 500 hPa geopotential heights*[a]

	El Niño	La Niña	Boundary condition mean
Zonal flow	Z_{i11}	Z_{i21}	
	T_{11}	T_{21}	T_{r1}
	μ_{11}	μ_{21}	μ_{r1}
Meridional	Z_{i12}	Z_{i22}	T_{r2}
flow	T_{12}	T_{22}	μ_{r2}
	μ_{12}	μ_{22}	
Initial condition	T_{c1}	T_{c2}	T
mean	μ_{c1}	μ_{c2}	μ_T

[a]Five different zonal and meridional flow initial conditions simulations are represented by Z_{ijk}, the arithmetic sum within the cell is represented by T_{jk}, and the mean of the sample within a cell is represented by μ_{jk}. The seasonal means for both initial and meridional conditions are shown in the bottom row (T_{ck}) and the seasonal means for the two phases of ENSO (T_{rk}) are shown in the right hand column. T is the grand total of all experiments, and μ_T is the overall mean.

midlatitude flow configuration (zonal or highly meridional) and to the tropical Pacific SST perturbation (El Niño or La Niña). The basic features of AGCM2 are described by McFarlane et al. (1992). Briefly, it is a spectral model with a triangular truncation of T32 in the horizontal resolution. It has a hybrid vertical coordinate with 10 levels, and employs a semi-implicit time step technique with a time step of 20 min. The model contains a comprehensive package of physical paramatrization of sub-grid scale processes.

For each SST forcing in the tropical Pacific (El Niño and La Niña), an ensemble of 10 integrations is performed with the model, five for the initial zonal flow and five for the initial meridional flow conditions. Thus, a total of 20 integrations are carried out (see Table 1). Each integration starts from 1 November and terminates at the end of February of the following year. We focus on the model results for December, January and February as the wintertime atmospheric response to the seasonally evolving warm and cold tropical Pacific SST forcing. Analysis of the equilibrium state of various atmospheric variables (such as the globally averaged kinetic energy) reveals that the model takes a few weeks to spin up. Therefore, to avoid this problem the model output for the first month (November) of the simulation is not analyzed. This choice also allows the land surface processes in the model to adjust from their initial climatological state.

Climatological SST forcing for El Niño (warm) is calculated as a composite of six El Niño events (1957–58, 1965–66, 1972–73, 1982–83, 1991–92, 1997–98). A composite of five La Niña events (1955–56, 1970–71, 1973–74, 1975–76, 1988–89) constitute La Niña (cold) SST forcing. Although global SST anomalies of the ENSO years were used as a boundary condition in the model simulations, it is noted that the main contribution to the midlatitude circulation variability originates from the tropical Pacific Ocean (Peng et al., 2000). Support for this statement comes from studies by Barsugli and Battisti (1998), who showed that extratropical SST anomalies arise mainly through heat flux related to the overlying anomalous atmospheric circulation. It has also been suggested that the extratropical SSTs could be forced by the tropical SSTs through the 'atmospheric bridge' (Lau and Nath, 1994). These SST anomalies have a smaller effect on the midlatitude atmospheric variability. Figure 1a shows the composite of SST anomaly for El Niño years for the Dec–Jan–Feb period; Figure 1b shows the same, but for La Niña. SST and sea-ice extent data were prescribed from the Hadley Centre GISST (Parker et al., 1995), with the exception of the 1997–98 (El Niño) case, for which the data were obtained from NCEP (National Center for Environmental Prediction) (Reynold and Smith, 1994). The composite monthly mean SST data were first interpolated to the model 96 × 48 Gaussian grid and then linearly interpolated (preserving monthly means) in order to obtain SST values at the model time step of 20 min. For each integration, either the El Niño or La Niña time-evolving SSTs then provide boundary forcing from the beginning of November of a particular year to the end of February of the following year. For each of the 10 ensemble integrations associated with either the El Niño or La Niña SST forcing, the only difference is the initial atmospheric configuration at the start of the model run.

The initial atmospheric flow conditions are categorized as either zonal or merdional. The categorization is performed subjectively by examining the average of the first 10 d in November of each year from 1960 to 1990 of the NCEP reanalysis (Kalnay et al., 1996) 500 hPa geopotential height field. For each of the two SST forcings, five zonal (1968, 1971, 1972, 1978, 1982) and five meridional (1962, 1966, 1970, 1976, 1986) conditions are chosen. These samples are chosen irrespective of ENSO events, and only 1982 (El Niño) and 1970 (La Niña) are associated with ENSO events. Both zonal and meridional flow configurations are

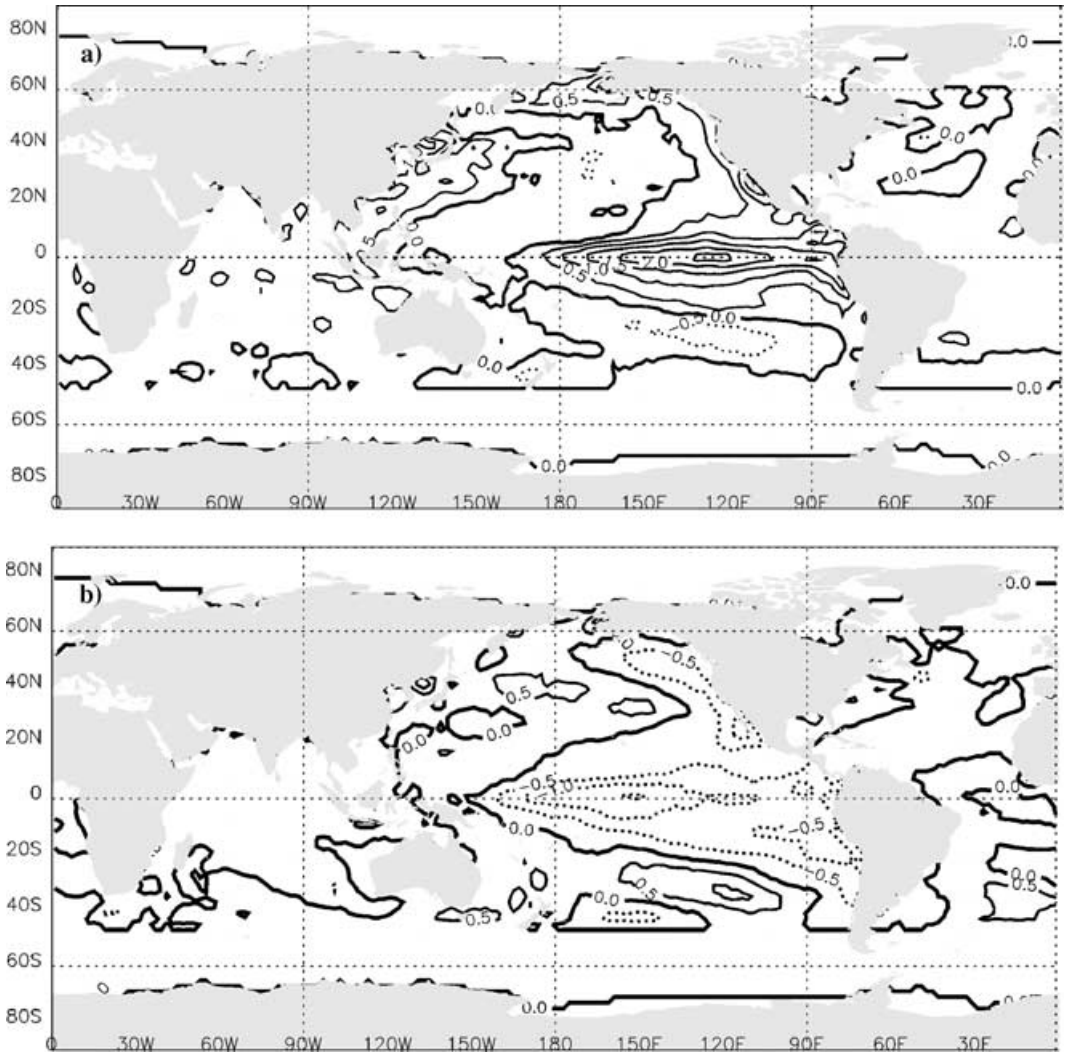

Fig. 1. Composite of sea surface temperature anomaly for Dec–Jan–Feb. The contour interval is 0.5 °C. (a) El Niño and (b) La Niña. The zero line is thickened. See text for years of composite.

subjectively chosen to represent the extreme flow conditions in order to enhance the possibility of obtaining a statistically significant signal of any effect due to changes in the atmospheric flow regime at the beginning of the winter season. The mean 500 hPa geopotential height and the anomaly fields over the Northern Hemisphere that reflect the zonal or the meridional nature of the initial flows over the PNA sector are shown in Figs. 2a and b and Figs. 2c and d, respectively. The anomaly is calculated relative to the 1968–1996 base period.

3. Methodology

The interannual variability of simulated 500 hPa geopotential heights is examined and intercompared using the statistical technique of two-way analysis of variance (ANOVA). A two-factor model is employed, similar to that used by (i) Zwiers (1996) to study interannual variability and identify locations of potential predictability in an ensemble of AMIP (Gates, 1992) climate simulations, (ii) Wang and Zwiers (1999) to examine interannual variability

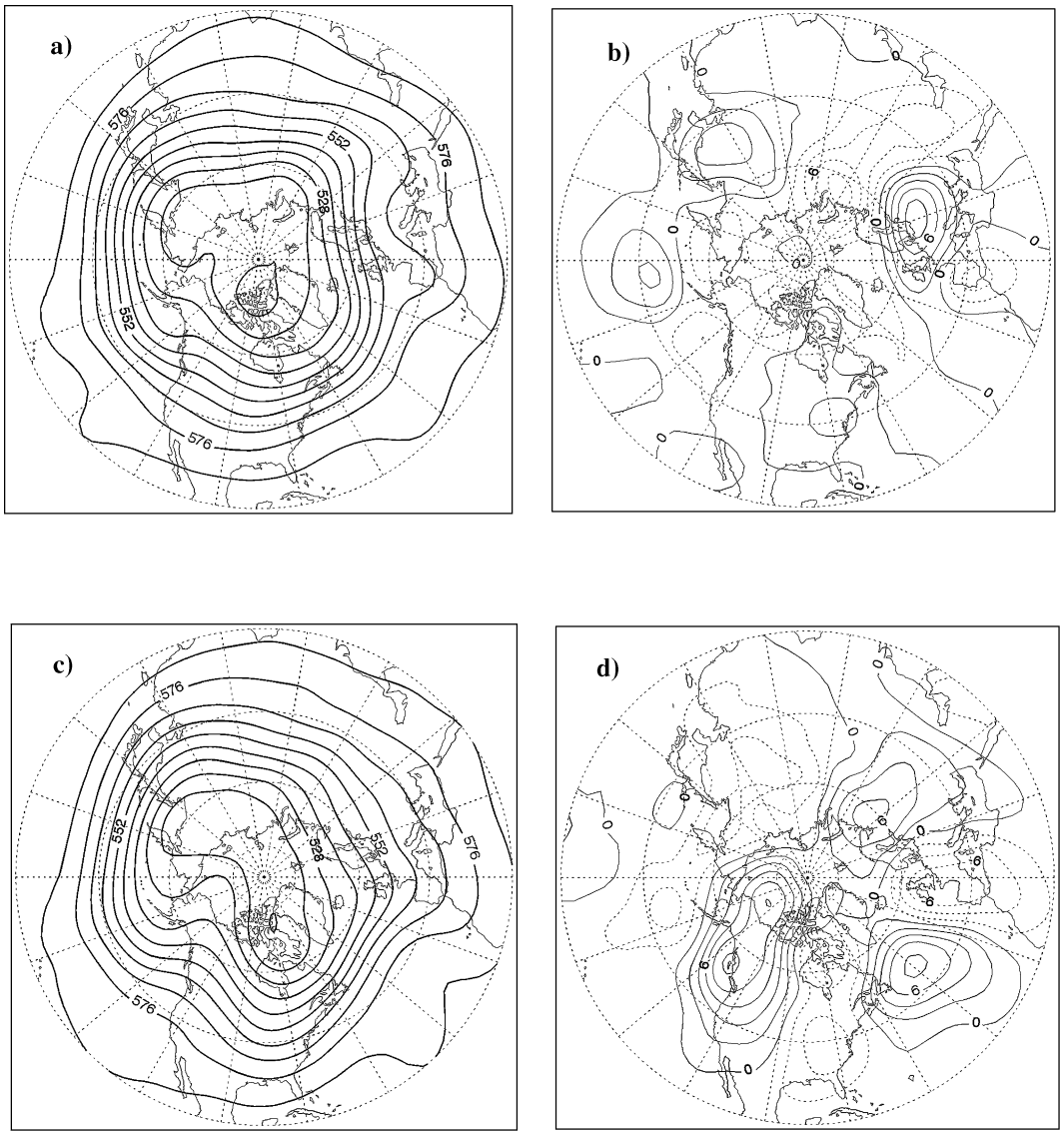

Fig. 2. Composite of the first 10 d of November of 500 hPa geopotential heights in decameters (Dm) from NCEP reanalysis used as initial flow configuration. (a) Zonal flow mean, (b) zonal flow anomaly, (c) meridional flow mean and (d) meridional flow anomaly. The contour interval is 12 Dm in (a) and (c), and 2 Dm in (b) and (d).

of precipitation in an ensemble of AMIP climate simulations and (iii) Zwiers et al. (2000) to isolate the effects of boundary conditions in an ensemble of climate simulations. All of these investigations employed the same AGCM2 as used in this study. Using the first version of the Hadley Centre Atmospheric Model (HADAM1), Rowell (1998) also used ANOVA to assess potential seasonal predictability with an ensemble of multidecadal GCM simulations. Since the ANOVA technique is well documented in the above studies, only a brief overview is given here. Further statistical discussions on ANOVA can be found in textbooks by Rice (1995), Searle et al. (1992) and Scheffe (1959).

The main objective is to partition the total variation of 500 hPa geopotential heights into two statistically

independent components that isolate (a) the variability forced by the prescribed ENSO SSTs and sea-ice extents and (b) the variability associated with the changes in the initial flow configuration (i.e. zonal or meridional over the PNA sector).

In order to apply the model it is necessary to assume that the observed 500 hPa geopotential height Z is Gaussian. An objective measure (Kolmogorov–Smirnov statistics) was used to test the goodness-of-fit of the Gaussian distribution, and the results showed little evidence contrary to the Gaussian assumption.

ANOVA partitions the total sum of squares SS_{tot} into four components,

$$SS_{\text{tot}} = SS_{\text{sst}} + SS_{\text{flow}} + SS_{\text{sxf}} + SS_{\text{inter}} \tag{1}$$

$$SS_{\text{tot}} = \sum_{ijk} \left[z_{ijk}^2\right] - \frac{T^2}{N} \tag{2}$$

$$SS_{\text{sst}} = \sum_{\text{col}} \left[\frac{T_{ck}^2}{n_{\text{c}}}\right] - \frac{T^2}{N} \tag{3}$$

$$SS_{\text{flow}} = \sum_{\text{row}} \left[\frac{T_{rk}^2}{n_{\text{r}}}\right] - \frac{T^2}{N} \tag{4}$$

$$SS_{\text{inter}} = \sum_{\text{jk}} \left[\frac{T_{jk}^2}{n}\right] - \frac{T^2}{N} \tag{5}$$

$$SS_{\text{sxf}} = SS_{\text{inter}} - SS_{\text{sst}} - SS_{\text{flow}} \tag{6}$$

where Z_{ijk} is the observed 500 hPa geopotential height, $n = 5$, n_{c} and $n_{\text{r}} = 10$ and $N = 20$, $i = 1, 5$ (choice of five initial conditions), $j = 1, 2$ (choice of ENSO phase), $k = 1, 2$ (choice of zonal or meridional flow regime). See Table 1 for explanation of various terms in eqs. (2)–(5).

SS_{sst} measures differences between the warm and cold phases of ENSO (i.e. boundary forcing effects), SS_{flow} measures differences between the two initial flow configuration, SS_{sxf} measures the interaction between the boundary forcing and initial flow configuration effects, and SS_{inter} is the variation from internal sources that remains after the effects of boundary forcing, initial conditions and interaction terms are taken into account. SS_{sxf} attempts to measure the influence that the initial flow configuration has on the ENSO response over the region under investigation. The total number of degrees of freedom df_{tot} is given by

$$df_{\text{tot}} = df_{\text{sst}} + df_{\text{flow}} + df_{\text{sxf}} + df_{\text{inter}} \tag{7}$$

where df_{sst}, df_{flow}, df_{sxf} and df_{inter} are the degrees of freedom associated with the boundary forcing, initial flow configuration, interaction and the remaining internal variability term effects, respectively.

A schematic representation of the collection of mean 500 hPa geopotential height due to boundary forcing and initial flow effects at each grid point is shown in Table 1. Statistical tests can be devised to test hypotheses about the various effects. Sums of squares due to various effects are divided by their respective degrees of freedom to obtain mean squares due to those effects. These mean squares are then tested against the mean square from internal sources to assess significant boundary and initial flow effects, as well as the interaction between the two effects.

A hypothesis-testing procedure helps us to decide whether the observed differences among the seasonal means are due to variations in independent variables or whether they might arise from chance factors. The null hypotheses for the three effects are set as follows:

(a) H_{sst}: $\mu_{\text{c1}} = \mu_{\text{c2}}$
El Niño and La Niña has no effect on the 500 hPa response.
(b) H_{flow}: $\mu_{\text{r1}} = \mu_{\text{r2}}$
Zonal or meridional flow configuration has no effect on the 500 hPa response.
(c) H_{sxf}: $(\mu_{11} - \mu_{12}) = (\mu_{21} - \mu_{22})$
ENSO response is not influenced by the initial flow configuration.

Variance ratios given by the Fisher F-statistics with the appropriate degree of freedom are then used to either accept or reject the null hypotheses. To test the null hypothesis that the prescribed boundary conditions do not influence the interannual variability, an F-ratio is formed:

$$F_{\text{sst}} = \frac{SS_{\text{sst}}/df_{\text{sst}}}{SS_{\text{inter}}/df_{\text{sst}}df_{\text{inter}}} \tag{8}$$

It is then the case that if a particular null hypothesis is true, the corresponding mean square will be an estimate of the variance given by the internal mean square. When H_{sst} is true, we would expect F_{sst} to take values near unity. F_{sst} will be greater than unity when H_{sst} is false. H_{sst} is tested by comparing F_{sst} with the critical value $F_{1-\alpha}[df_{\text{sst}}, df_{\text{sst}}\, df_{\text{inter}}]$, where α represents the selected significance level and the notation $F_{1-\alpha}[m, n]$ denotes the $(1 - \alpha)$ quantile of F distribution with m, n degrees of freedom. An unbiased estimator of the proportion of the total variance due to boundary-forced effects is (Rowell, 1998)

$$p_{\text{sst}} = \frac{SS_{\text{sst}} - (SS_{\text{inter}}/df_{\text{inter}})}{SS_{\text{tot}}}. \tag{9}$$

Similarly, the null hypothesis, that the initial flow conditions do not affect intersimulation variability, can be tested by comparing

$$F_{\text{flow}} = \frac{SS_{\text{flow}}/df_{\text{flow}}}{SS_{\text{inter}}/df_{\text{flow}}df_{\text{inter}}} \tag{10}$$

with $F_{1-\alpha}[df_{\text{flow}}, df_{\text{flow}}df_{\text{inter}}]$; an unbiased estimator of the proportion of the total variance arising from the initial flow effects is

$$p_{\text{flow}} = \frac{SS_{\text{flow}} - (SS_{\text{inter}}/df_{\text{inter}})}{SS_{\text{tot}}}. \tag{11}$$

Analogous F-statistics were formulated in order to test for the effects of the interaction null hypothesis. A more detailed description of the analysis scheme employed here can be found in Rowell (1998).

4. Results

4.1. Integration variability

Figure 3(a) shows the wintertime (Dec–Jan–Feb) ENSO variability of the 500 hPa geopotential height field, calculated as the standard deviation of the combined ensemble of 20 integrations for the Dec–Jan–Feb period from the zonal and meridional cases. There is a variability maximum with a centre of over 70 m located over the North Pacific at 45°N, 155°W. Another region of maximum variability connects a centre in western Canada to a centre over southern Greenland. The simulations also show an area of relatively low variability from the southern United States through the Great Lakes into the North Atlantic.

The model variability is compared with that derived from NCEP reanalysis data for the 19 moderate to

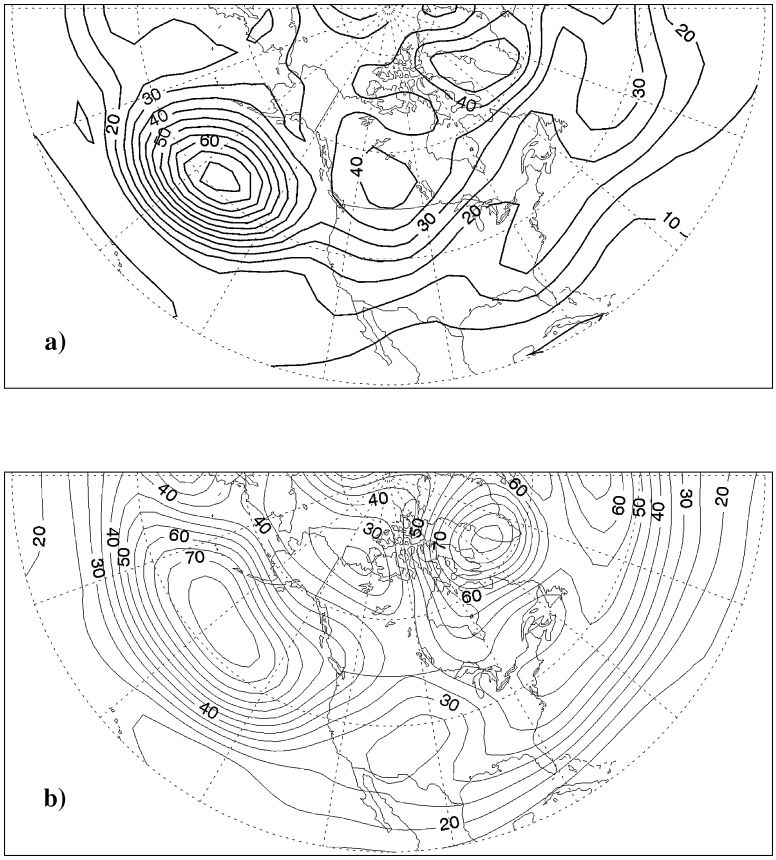

Fig. 3. Standard deviation of (a) model simulated and (b) based on NCEP/NCAR reanalysis 500 hPa geopotential heights in meters for Dec–Jan–Feb for 20 ENSO cases corresponding to 10 zonal and 10 meridional flow regimes. The contour interval is 5 m.

strong ENSO winters during the 1958–98 period in Fig. 3(b). The standard deviation is calculated for the Dec–Jan–Feb period. Although the simulations reproduce the overall features of the observed variability, there are some noticeable differences. The observed variability associated with the Gulf of Alaska centre is slightly stronger and more extensive than the simulated variability. Also, the centre of variability over southern Greenland is much stronger (nearly double the simulated value) and slightly displaced westward in the NCEP data. The relative maximum centre over western Canada as revealed by the model is not found as a separate entity in the NCEP data. Rather, two relative minimum centres are present (one over the southwestern United States and another over the Beaufort Sea) in the observed data. Compared with the simulated data, the NCEP data also show stronger variability in the 500 hPa circulation over the Great Lakes region. Overall, the amplitude of the wintertime variability in the ENSO simulations are somewhat attenuated compared to those found in the observed data set. Using the same atmospheric model, Zwiers et al. (2000) also found similar behaviour in their AMIP simulation.

Other climate models also have varying degrees of difficulty in emulating midlatitude circulation adequately. For example, Wang and Fu (2000) recently examined the variability of the PNA pattern with the National Center for Atmospheric Research Community Climate Model (NCAR CCM3) that was forced with the observed time-varying tropical SSTs. Their results showed that the ensemble model circulation does not sufficiently replicate the observed timing of the midlatitude circulation during El Niño episodes.

Notwithstanding these differences, it is believed that the simulations from AGCM2 are capable of providing useful information about the dependence of midlatitude circulation evolution on the tropical Pacific SSTs and the initial flow configuration. Although the model-produced variability is weaker than observed, the overall agreement in the pattern of variability is sufficiently encouraging to proceed with the study objective.

In the remainder of this paper, the ANOVA technique will be used to partition the model variability into those components ascribable to the boundary-forced effects and those to the initial flow condition effects. The ANOVA technique allows for a clean statistical separation of the total variance as induced by the time-varying SSTs from that induced by the initial flow configuration. Based on the above observations, it should be noted that the model-produced variance would be an underestimate of the true variance.

4.2. *Boundary-forced interannual variance*

The boundary-forced effects are strong in the tropics and become weaker in the midlatitudes where internal variability is large relative to the signal from the slowly varying boundary forcing. From the potential predictability point of view, it is of interest to know the proportion of total variance that can be accounted for by the boundary conditions. Figure 4(a) shows the proportion of boundary-forced variability of Dec–Jan–Feb mean 500 hPa geopotential heights at each grid point as revealed by ANOVA over the PNA sector. Not surprisingly, significant boundary-forced effects are evident over a large area of the sector. The pattern of significance resembles the PNA teleconnection pattern as shown by Barnston and Livezey (1987). The null hypothesis that the boundary-forced effects do not contribute to the overall variability can be rejected at the 5% significance level over a large area of investigation. Nearly 54% of the area exhibits statistical significance at the 5% level (Livezey and Chen, 1983). While performing a similar type of analysis with GCMs, Rowell (1998) also found significant contribution from the slowly varying boundary conditions in the PNA centres of actions.

The atmospheric response to the boundary-forced effects of ENSO is, for the most part, deterministic (Wang and Fu, 2000). Therefore the boundary-forced component of the total sum of squares can be regarded as a squared difference between two ensemble means, and the F-test used here can also be interpreted as the square of the Student t-test that asks whether the mean warm phase climate is different from the mean cold phase climate.

To examine the boundary-forced effects for the individual winter months, ANOVA is repeated on December, January and February individually. Figures 4b–d show that the null hypothesis of no effect can be rejected over 30%, 38% and 47% for the three individual months, respectively. These maps show that the PNA-like teleconnection pattern starts to manifest itself in December with well organized centres south of the Aleutian Islands and over southern Canada and northern United States. It is not until January (Fig. 4c) that a weak centre appears over the southeastern United States. By February (Fig. 4d), a classical PNA teleconnection pattern with three main centres of action is evident over the PNA sector.

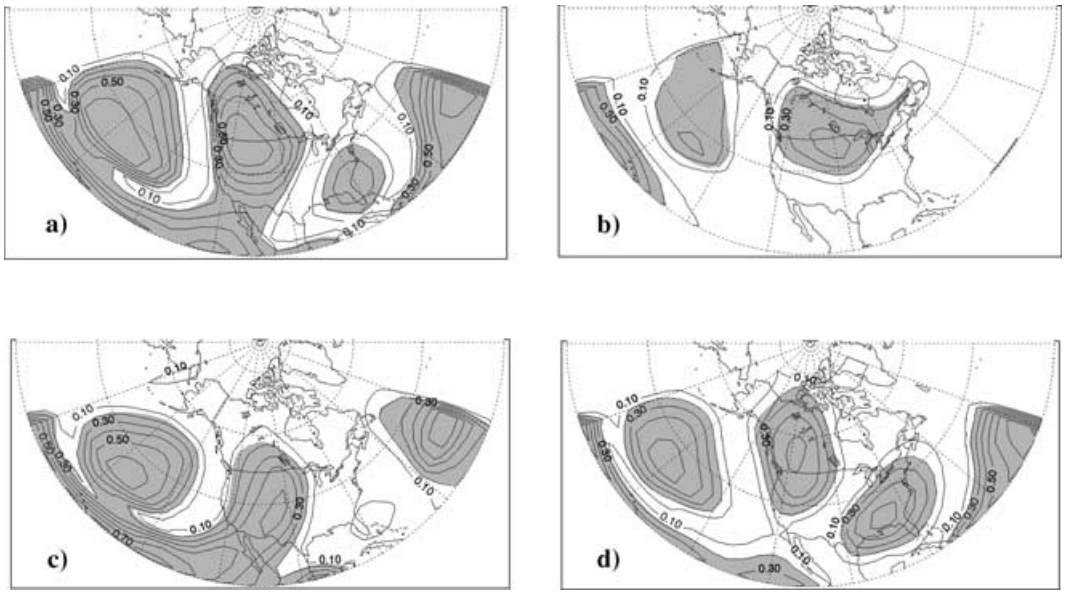

Fig. 4. Ratio of boundary-forced variance to the total variance for 500 hPa geopotential heights as derived by ANOVA. The contour interval is 0.10. The significant F-ratio at the 5% level of significance is indicated by shading. (a) Dec–Jan–Feb, over 54% of the area the null hypothesis of no boundary effect can be rejected at the 5% level of significance, (b) December, 30% of the area exhibit statistical significance at 5%, (c) January, 38% of the area exhibit statistical significance at 5% and (d) February, where 47% of the area show statistical significance at 5%.

While examining the evolution of the PNA pattern in the NCEP reanalysis dataset, Wang and Fu (2000) also found that during El Niño years the PNA pattern tends to occur more frequently in late winter (Jan–Mar) than in the early winter months (Nov and Dec).

The results shown in Fig. 4 are consistent with seasonal forecast skill as demonstrated by dynamical and statistical forecasting systems (Derome et al., 2001; Barnston, 1994). In summary, the analysis of the AGCM2 results show that specified SSTs and sea-ice boundary conditions induce a significant amount of midlatitude circulation variability in both seasonal and monthly means, and the pattern of variability strongly resembles the PNA teleconnection.

Straus and Shukla (2000) carried out a number of simulations with the Center for Ocean–Land–Atmosphere Studies (COLA) GCM in which tropical SSTs were specified as a boundary condition. The authors claimed that the resulting midlatitude circulation variability pattern is quite distinct from the PNA pattern, and more closely resembles the Tropical/Northern Hemisphere (TNH) pattern (Barnston and Livezey, 1987). The structure of our boundary-forced pattern, shown in Fig. 4, more vividly resembles the PNA pattern, and is quite similar to the pattern of seasonal skill produced from the NCEP-MRF9 model (Peng et al., 2000). These observations raise the issue of the dependent role played by various models on the structure of boundary-forced midlatitude variability.

4.3. Variance ascribed to initial flow configuration

Will variations in the initial flow configuration lead to significant inter-simulation variation? The experimental setup and the ANOVA technique used in this study allow us to answer this question with some certainty. Displayed in Fig. 5 are the F-statistics which are used to test whether the initial flow configuration affects the winter mean geopotential heights. The null hypothesis that the initial flow configuration does not contribute additional variance is rejected at the 10% level of significance over 34% of the PNA sector for the Dec–Jan–Feb period (Fig. 5a). The 5% level of significance covers about 21% of the region. The pattern of statistical significance for the initial flow configuration is strongly suggestive of the PNA teleconnection, although much weaker than that obtained from the boundary condition effects. This pattern is very

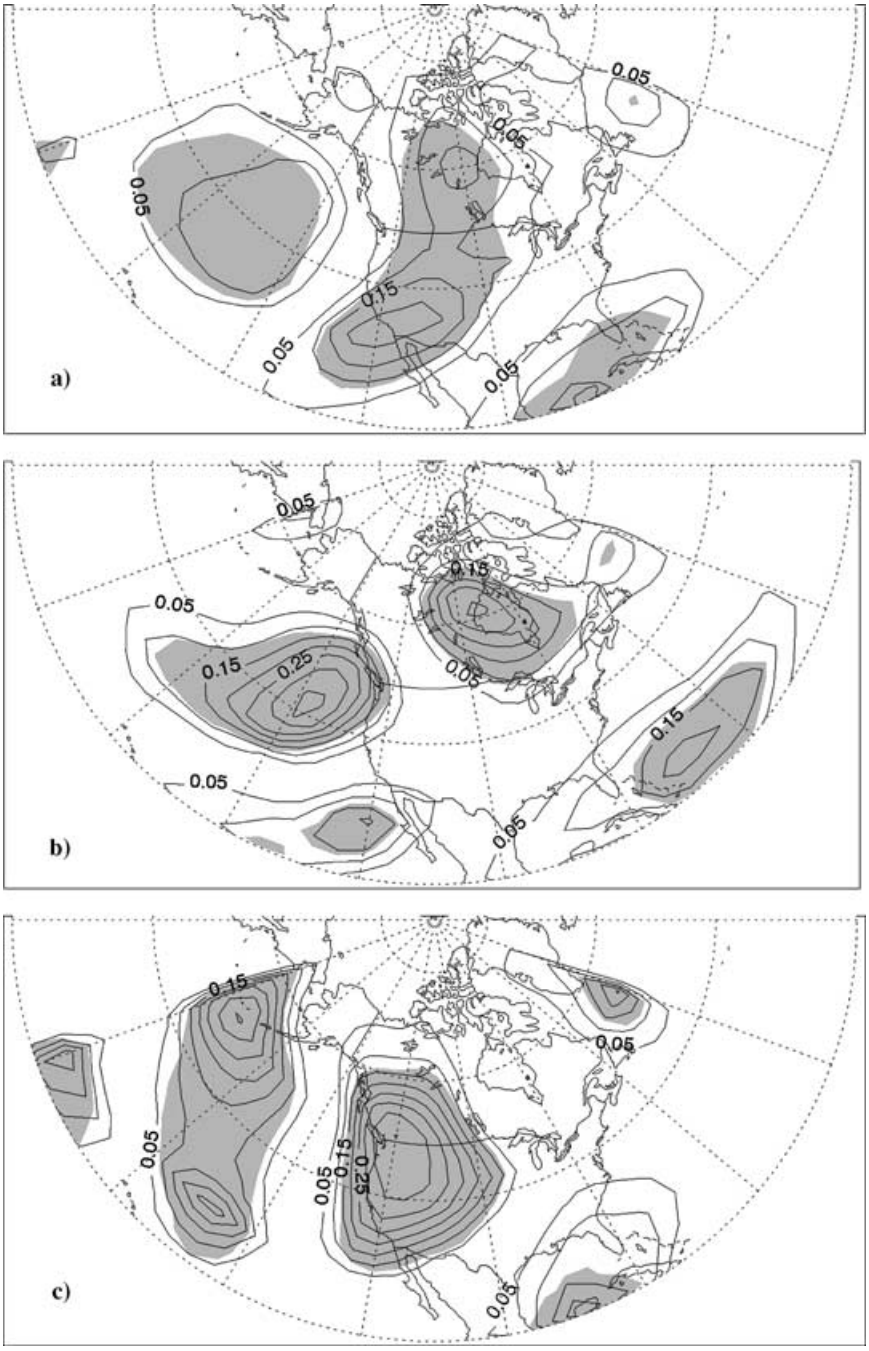

Fig. 5. Ratio of initial flow condition variance to the total variance for 500 hPa geopotential heights as derived by ANOVA. The contour interval is 0.05. The significant *F*-ratio at the 10% level for the initial flow effect is indicated by shading. (a) Dec–Jan–Feb, over 34% of the area the null effect of no initial flow effect can be rejected at the 10% level of significance; (b) December, 19% of the area exhibit statistical significance at 10%; (c) January, where 23% of the area exhibit statistical significance at 10%.

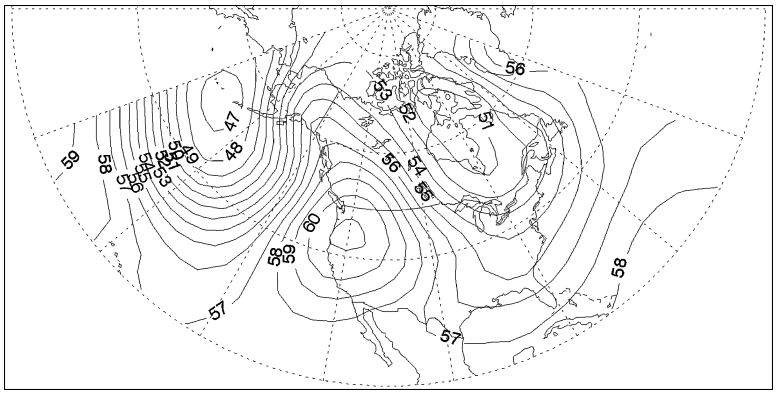

Fig. 6. Difference in 500 hPa geopotential. heights between the mean of 10-member zonal and the mean of 10-member meridional flow model simulation over the Pacific North American sector for January. The contour interval is in meters. The pattern is similar to the PNA pattern.

similar to the internal variability pattern found by Straus and Shukla (2000).

In order to examine the effects of the initial flow conditions on the midlatitude circulation for the individual months, the ANOVA technique is applied to December and January data. Figures 5b and c display the variance explained over Pacific North America. The null hypothesis of no effect can be rejected at the 10% level of significance over 19% of the area for December and 23% for January (indicated by shading). A PNA-like pattern can be identified in December (Fig. 5b), and the pattern takes a more classical PNA appearance in January (Fig. 5c). During February (not shown), the variance explained is rather small and none of the area shows significance. It would appear that the initial flow effects are the strongest in January, but virtually disappear in February.

The relationship between the zonal and meridional flow in the model is further analyzed by forming differences in the mean of 10-member zonal and 10-member meridional flow regimes for each month of the simulation. Results show no discernable pattern in the difference maps in December or February (neither is shown). A teleconnection pattern very similar to a PNA-like pattern, however, emerges in January (Fig. 6). This reinforces the results shown in Fig. 5. There may be a number of physical or dynamical reasons for the January pattern. One of them could be the nature of the air-sea interaction in the North Pacific Ocean for each of the two initial flow regimes. The atmosphere would likely evolve in a more predictable manner for one initial flow regime than the other.

To demonstrate that the patterns shown in Fig. 5 are robust, ANOVA is performed on a smaller ensemble of size three. There are 10 different ways of selecting three samples from the original five samples for each of the two initial conditions, making 100 different combinations of initial flow conditions possible. If the PNA pattern remains identifiable when the signal-to-noise ratio is reduced in the smaller ensemble, then the existence of the initial flow effects cannot be ruled out unequivocally. Figure 7 shows the frequency of pattern correlation between the original five-sample variance map and those obtained from the smaller three ensemble runs for the individual months. It is clear that the initial flow effects are evident during December (Fig. 7a). About 60% of the sample runs correlate at 0.6 or higher with the original pattern. The effect becomes more prominent during January (Fig. 7b) when about 80% of the sample runs correlate at 0.6 or higher. The effects break down in February (Fig. 7c) as most of the correlations are below the 0.6 threshold. These results provide further corroborating evidence of the existence of significant initial flow effects on the midlatitude atmospheric circulation.

The initial flow effects in Fig. 5 are also not the artefacts of the differential drift in the model for the two initial flow conditions. To discount the possibility of model drift happening differently for the two kinds of initial flow conditions, mean-February minus mean-December differences for the two kinds of flow conditions are computed. A statistical test is used to check zonal minus meridional difference (δ) between these differences. It was found that δ was not

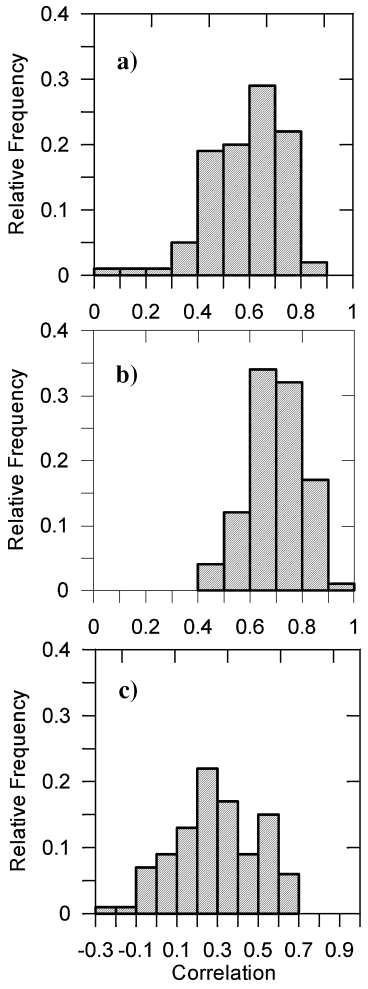

Fig. 7. Relative frequency of the pattern correlation between the one five-member and 100 three-member ensembles for the initial flow effect. (a) December, (b) January and (c) February. Over 80% of the correlations are higher than 0.6 in January. Note the difference in scale in (c).

significantly different from zero at the 5% level of significance. The combined evidence of no differential model drift and of the robustness of the patterns shown in Fig. 7 lends credence to the reality of the initial flow effect.

Previous experiments with AGCM2, under the AMIP protocol for the period 1979–88, have shown that the initial conditions do not induce any additional variability (Zwiers, 1996). In those experiments, the initial state was specified once (from the operational analysis) at the beginning of a 10-yr run. In contrast, both the length of the integration and the configuration of the initial states are different in the current study. Two diametrically opposite flow configurations are used to represent the initial state of each 4-month run. Expectations for information conveyed by the initial state are much different for the two kinds of experiments. It would appear that the model ascribes a fair amount of variability to the initial flow configuration chosen here. It is suggested that other processes, such as the air-sea interaction in the northern oceans (Sheng, 1999), the configuration of the north Pacific SSTs (Lee et al., 2002), as well as the atmospheric internal variability, may contribute to the circulation variability over the PNA sector.

The fact that processes other than ENSO can also contribute to the variability of the PNA pattern is backed by other studies. While analyzing 44 years of winter data from the operational model output of the European Centre for Medium Range Forecasting, Renwick and Wallace (1996) found that about 30% of the PNA occurrences are not associated with the ENSO cycle. Additional support for the robustness of the PNA pattern (other than from boundary conditions) comes from Esbensen (1984). Through digital filtering analysis, it was found that the PNA pattern of variability manifests itself on various timescales from intermonthly to interannual.

The ANOVA technique reveals no significant contribution from the interaction between the boundary-forced SSTs and the initial flow configuration effects. No coherent areas of statistically significant effect due to the interaction term are found either for the individual winter months or for the season as a whole. Thus, no dynamical interaction between the PNA mode of variability associated with the ENSO SST perturbations and that associated with the initial atmospheric flow anomaly is found. This suggests that the relative contributions from the SST and the initial flow effects are linearly independent and additive.

4.4. Patterns of spatial variability

Modes of variability that contribute most strongly to the patterns shown in Figs. 4 and 5 are isolated with an EOF analysis for the Dec–Jan–Feb period for the Northern Hemisphere north of 20°N. Figure 8 shows the first two EOFs from the model simulations. A rather well defined PNA-like pattern is evident in EOF1 (Figure 8a) for the Dec–Jan–Feb period. EOF2 (Fig. 8b) is a mixture of the North Atlantic Oscillation

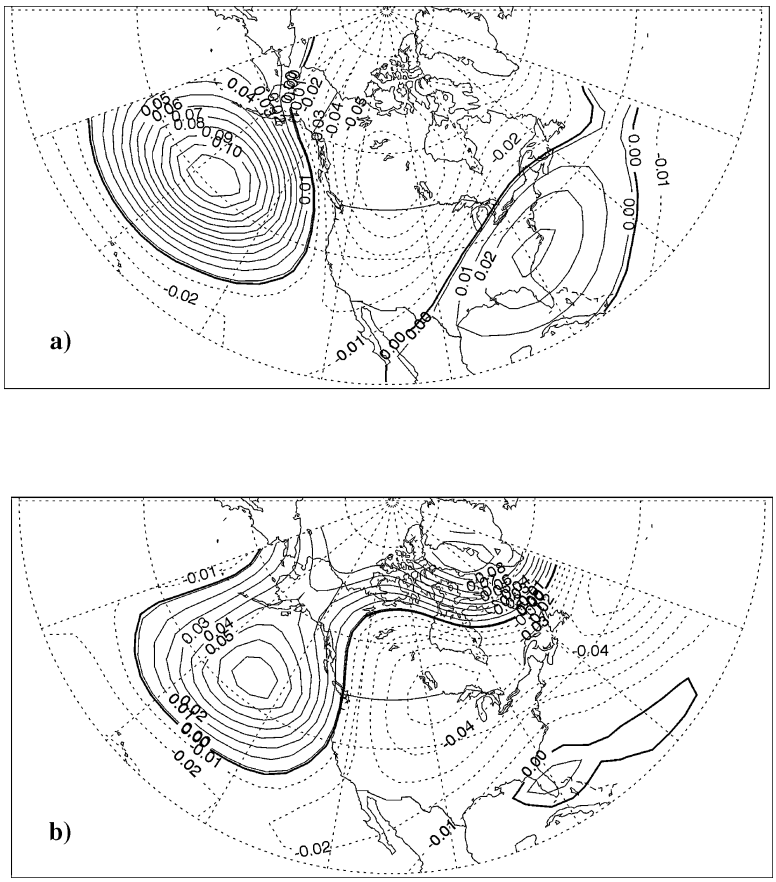

Fig. 8. (a) EOF1 for Dec–Jan–Feb of 500 hPa geopotential heights as derived from model ensemble. EOF1 shows the PNA mode of the Northern Hemisphere variability and explains over 50% of the seasonal variability. (b) EOF2 of the same field. EOF2 shows a mixture of the North Atlantic Oscillation (NAO) and the PNA modes and explains about 17% of the seasonal variability. The contour interval is 0.01. The signs are arbitrary and units are dimensionless.

(NAO) and the PNA (Barnston and Livezey, 1987). The leading two EOFs account for 68% of the total variance. The third EOF (not shown) explains a considerably smaller proportion of the variance. To identify patterns of spatially coherent variability emanating from the boundary-forced effect and from the initial flow configuration, 500 hPa geopotential heights were reconstructed from the two leading EOFs. ANOVA is repeated on the reconstructed heights over the PNA sector. Results shown in Fig. 9a confirm highly significant boundary-forced effects over a large part of the sector. Over 83% of the area the null hypothesis of no effect can be rejected at the 5% level of significance. Moreover, the boundary effect has a strong signature in the PNA mode of variability. The initial flow effect on the reconstructed heights also shows statistical significance. The null hypothesis of no effect can be rejected over 61% (30%) of the sector at a 10% (5%) level of significance (Fig. 9b). Again, locations showing significance form the centres of a PNA-like pattern. Thus, it would appear that the PNA mode of variability plays a central role in explaining the variability that can be ascribed to both the boundary and initial flow effects. In order to reinforce the above findings, ANOVA was performed on the amplitude time series of EOF1 (PC1) and EOF2 (PC2) separately. The amplitude of the leading Dec–Jan–Feb mode (the PNA mode) is significantly affected by the boundary forcing (even at the 1% level of significance). The initial flow effects are also significant in the ensemble at the 5%

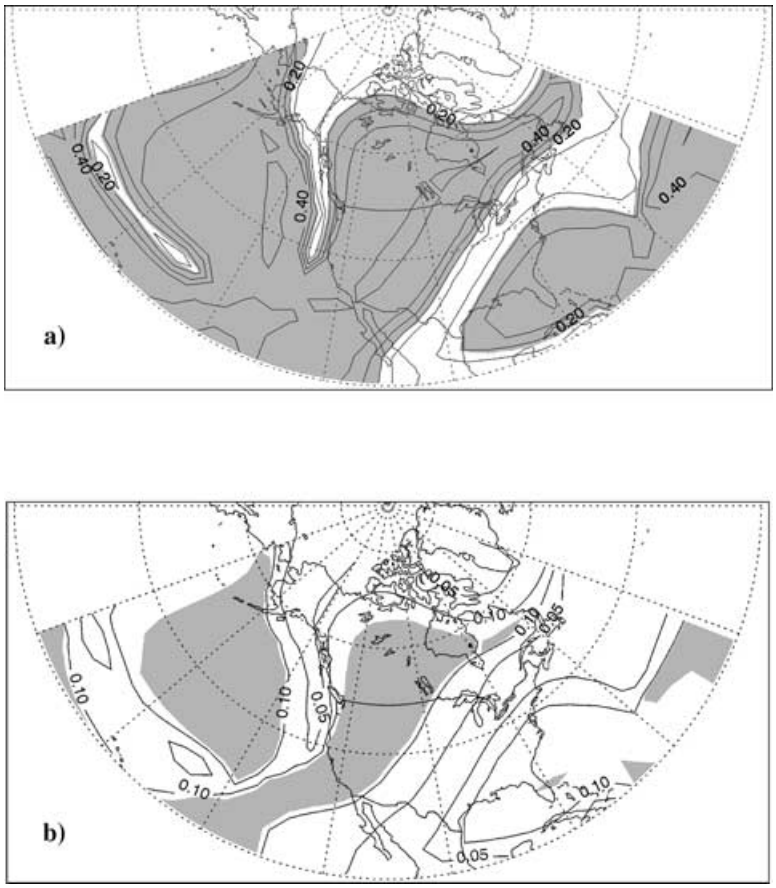

Fig. 9. *F*-Ratio of the Dec–Jan–Feb 500 hPa geopotential heights as reconstructed from EOF1 and EOF2 for (a) the boundary-forced effect and (b) the initial flow condition effect. The contour interval is 0.1 in (a) and 0.05 in (b). The shaded area shows statistical significance at 5% for the boundary-forced effect, where over 83% of the area the null hypothesis of no effect can be rejected. For the initial flow condition, significance is determined at 10%, and over 61% of the area, the null hypothesis of no effect can be rejected.

level of significance. In Figs. 5 and 7 it was shown that the initial flow effects are prevalent in December and January but break down in February. These findings are confirmed in the ANOVA analysis of the PCs of the individual month EOFs. In PC1, the boundary-forced response is strong and statistically significant for December, January and February. The initial flow effect, however, is evident in December and more clearly so in January, but is virtually non-existent in February. The amplitude of the second (Dec–Jan–Feb) mode is apparently not affected by either the boundary or the initial flow configurations in the AGCM2 ensembles, indicating that EOF2 is mostly related to other model's internal variability. Overall, the PNA mode of variability in AGCM2 has been found to be most sensitive to the boundary-forced effect, and to a lesser extent to the initial flow configuration. The AGCM2 results are in agreement with observational studies of Shabbar and Khandekar (1996) and Mo et al. (1998) which showed that the PNA pattern dominates the winter climate variability over the PNA sector during moderate to strong ENSO years.

5. Summary and discussion

The primary intent of this study was to separate and quantify the contribution from boundary-forced

tropical SSTs and initial midlatitude flow configurations to the wintertime circulation anomalies over the PNA sector. One of the other objectives was to identify the modes of variability through which the effects of boundary and initial flow conditions are revealed over the PNA sector. Composites of time-evolving SSTs from six strong El Niño and five strong La Niña events and sea ice extent as prescribed by the GISST were used to specify lower boundary conditions in the model. Different flow configurations were chosen to portray initial conditions in the experiment. Two diametrically opposite flow configurations obtained from the NCEP reanalysis were specified at the start of the simulations.

The interannual variability of the 500 hPa geopotential heights in an ensemble of five simulations of the AGCM2 was analyzed by applying the standard two-way ANOVA technique at individual grid points over the PNA sector for the winter (Dec–Jan–Feb) season and for individual months. Consistent with the prescribed SSTs (either warm or cold phase of ENSO) and sea ice extent, the model produced five realizations corresponding to the initial zonal flow and five realizations corresponding to the meridional flow regime. Thus, there were 20 realizations to which the ANOVA technique was applied.

Consistent with previous studies, the model results show that the specified time-varying SSTs in the tropical Pacific and sea ice boundary contribute significantly to the circulation variability in the seasonal and monthly mean 500 hPa geopotential heights over the PNA sector. Moreover, the model faithfully reproduces the variability over North America as the PNA mode of variability. In an earlier version of the same model, Boer (1985) showed that the model's extratropical response to 1982–83 El Niño SST forcing resembled the observed circulation anomalies. More recently, Zwiers et al. (2000) used an ANOVA technique to show that AGCM2 can ascribe ENSO-related variability to the extratropical latitudes in a significant way.

The model results also show that the initial flow configuration induces additional variability over the region through a PNA-like mode of variability. The contribution from the initial flow configuration is significant at the 5% level over 21% of the area under investigation. Although small, this variability could arise from air–sea interaction in the North Pacific (Lee et al., 2002) as well as persistence of land surface processes over the PNA sector in ENSO years. The feedback of the extratropical SSTs on the atmosphere as documented by Saravanan (1998) and Bladé (1997) could also provide a possible explanation for the origin of the initial flow effect. These studies use an interactive ocean and show that the extratropical SST anomalies arise mainly through the heat fluxes related to the overlying atmospheric anomalies, and these SSTs in turn have a measurable feedback on the overlying atmospheric variability. It is also plausible that the initial configuration of the atmospheric circulation produces changes in land surface characteristics such as the nature of the snow cover. The resulting lower boundary condition may in turn affect the circulation variability a month or two later over North America. It is also found that the relative contributions from the tropical SSTs and the initial atmospheric flow configurations are linearly independent and additive.

In order to isolate the mode of atmospheric variability instrumental in producing the external and the internal sources of variability, the ANOVA technique was applied to the 500 hPa anomaly field filtered with the two leading EOFs. Results show that there was considerable boundary-forced and, to a lesser extent, initial-flow variability that was realized by the EOF filtered data. To further isolate the mode of variability responsible for the contribution, ANOVA was then applied to the time series of the amplitude (PCs) of the two leading Northern Hemisphere 500 hPa geopotential height EOFs in the ensemble.

The structure of midlatitude variability in AGCM2 from the SST-forcing and that from the initial flow conditions are very similar, and strongly resembles the PNA teleconnection. Straus and Shukla (2000) carried out a number of similar simulations in their COLA-GCM model and concluded that their SST-forced pattern is quite distinct from that produced by the internal variability of their model, which is more like the PNA teleconnection. They pointed to significant differences between the two patterns over western North America and the adjoining eastern Pacific Ocean, as well as a small region northeast of the Great Lakes. It is interesting to note that other investigators, in their GCM predictability experiments, have not found these differences. We also note that the SST-forced midlatitude skill pattern from the NCEP-MRF9 (Peng et al., 2000) produces a pattern very similar to that shown in Fig. 5. This raises the issue of model dependency on the SST-forced midlatitude variability, and the possibility that the SST-forced midlatitude variability from

different models may deviate from the classical PNA mode of variability.

Not surprisingly, the PNA-like mode of variability is found to contribute substantially to the boundary-forced effects; furthermore, the PNA teleconnection is also found to be the mechanism through which the initial flow configuration makes its contribution to the overall variability. These findings are in agreement with earlier investigations (e.g. Kumar and Hoerling, 1995, and Zwiers et al., 2000) where the PNA was also found to play a central role in communicating the tropical SST signal to the midlatitude atmosphere over North America.

This study underlines the ability of AGCM2 to produce a PNA-like pattern with both SST-forced and internal variability (through initial flow conditions). The results show that they both induce the PNA pattern. Other studies have shown that, unlike other modes of atmospheric variability, the PNA pattern is evident on a range of timescales. For example, Esbensen (1984) used digital filtering and spatial correlation analysis on 700 hPa geopotential height observed data to show that while some teleconnections are dominant on the intermonthly scale, and others are prevalent on the interannual scale, only the PNA pattern appears to be prominent in both the interannual and intermonthly signals. That the PNA teleconnection is produced from a number of sources is also supported in observational studies. In addition to the variability in the tropical Pacific, the genesis of the PNA pattern can be found from other sources. Blackmon et al. (1984) argued that forcing from a wide range of locations could excite the PNA pattern. They present evidence of poorly defined negative lag-correlation patterns with the base grid-point in the North Pacific, but stronger lag-correlation patterns for positive lags indicating strong dispersion of energy towards the downstream centres of actions of the PNA pattern. The exact mechanism through which the initial flow effects makes itself evident over Pacific North America remains somewhat elusive.

In this study, an ensemble size of five was chosen. This ensemble size is close to the six ensembles used in each of the two prediction models for the operational production of seasonal forecasts at the Canadian Meteorological Centre (Derome et al., 2001). Kumar and Hoerling (2000) argued that the seasonal predictability of the physical system has an upper bound, and that the maximum potential value of seasonal predictability can be realized with a modest seven-member ensemble.

The experimental design and the methodology employed here allowed for a clear separation of externally and internally induced variability in AGCM2. Furthermore, through EOF decomposition, the technique provided useful insight into the mode of atmospheric variability responsible for teleconnecting these different sources of variability to the PNA sector.

5. Acknowledgment

We thank Francis Zwiers for his helpful comments and valuable suggestions throughout the course of this study. Constructive criticisms from two anonymous reviewers are appreciated.

REFERENCES

Barnston, A. G. 1994. Linear statistical short-term climate predictive skill in the Northern Hemisphere. *J. Climate* **7**, 1513–1564.

Barnston, A. G. and Livezey, R. E. 1987. Classification, seasonality and persistence of low frequency atmospheric circulation patterns. *Mon. Wea. Rev*. **115**, 1083–1126.

Barsugli, J. J. and Battisti, D. S. 1998. The basic effects of atmosphere-ocean thermal coupling on midlatitude variability. *J. Atmos. Sci*. **55**, 477–493.

Blackmon, M. L., Lee, Y.-H., Wallace, J. M. and Hsu, H. H. 1984. Time variation of 500 mb height fluctuations with long, intermediate and short time scales as deduced from lag-correlation statistics. *J. Atmos. Sci*. **6**, 981–991.

Bladé, I. 1997. The influence of midlatitude ocean-atmosphere coupling on the low-frequency variability of a GCM. Part I: No tropical SST forcing. *J. Climate* **10**, 2087–2106.

Boer, G. J. 1985. *Modelling the atmospheric response to the 1982/83 El Niño. Coupled cean–atmosphere models*. Elsevier, Amsterdam, 1–17.

Derome J., Brunet, G., Plante, A., Gagnon, N., Boer, G. J., Zwiers, F. W., Lambert, S. J., Sheng, S. and Ritchie, H. 2001. Seasonal predictions based on two dynamical models. *Atmos-Ocean*. **39**, 485–501.

Esbensen, S. K. 1984. A comparison of intermonthly and interannual teleconnections in he 700 mb geopotential height field during the Northern Hemisphere winter. *Mon. Wea. Rev*. **112**, 2016–2032.

Fyfe, J. C., Boer, G. J. and Flato, G. M. 1999. The Arctic and Antarctic Oscillations and heir projected changes under global warming. *Geophys. Res. Lett*. **26**, 1601–1604.

Gates, W. L. 1992. The atmospheric model intercomparison project. *Bull. Am. Meteorol. Soc*. **73**, 1962–1970.

Geisler, J. E., Blackmon, M. L., Bates, G. T. and Munoz, S. 1985. Sensitivity of January climate response to the magnitude and position of equatorial Pacific sea surface temperature anomalies. *J. Atmos. Sci*. **42**, 1037–1049.

Hoerling, M. P. and Kumar, A. 1997. Why do North American climate anomalies differ from one El Niño event to another? *Geophys. Res. Lett*. **24**, 1059–1062.

Horel, J. D. and Wallace, J. M. 1981. Planetary-scale atmospheric phenomena associated with the Southern Oscillation. *Mon. Wea. Rev.* **109**, 813–829.

Hoskins, B. J. and Karoly, D. J. 1981. The steady linear response of a spherical atmosphere to thermal and orographic forcing. *J. Atmos. Sci.* 38, 1179–1196.

Kalnay, E. and co-authors 1996. The NCEP/NCAR 40-year reanalysis project. *Bull. Am. Meteorol. Soc*. **77**, 437–471.

Kok, C. J. and Opsteegh, J. D. 1985. On the possible causes of anomalies in seasonal mean circulation patterns during the 1982–83 El Niño event. *J. Atmos. Sci*. **42**, 677–694.

Kumar, A. and Hoerling, M. P. 1995. Prospect and limitations of seasonal atmospheric GCM predictions. *Bull. Am. Meteorol. Soc*. **76**, 335–345.

Kumar, A. and Hoerling, M. P. 2000. Analysis of a conceptual model of seasonal climate variability and implications for seasonal prediction. *Bull. Am. Meteorol. Soc*. **81**, 255–264.

Lau, N. G. and Nath, M. J. 1994. A modeling study of the relative roles of tropical and extratropical SST anomalies in the variability of the global atmosphere–ocean system. *J. Climate* **7**, 1184–1207.

Lee, E. J., Jhun, J. G. and Kang, I. S. 2002. The characteristic variability of boreal wintertime atmospheric circulation in El Niño events. *J. Climate* **15**, 892–904.

Livezey, R. E. and Chen, W. Y. 1983. Statistical field significance and its determination by Monte Carlo techniques. *Mon. Wea. Rev*. **10**, 111–127.

Lorenz, E. N. 1984. Irregularity: a fundamental property of the atmosphere. *Tellus* **36A**, 98–110.

McFarlane, N. A., Boer, G. J., Blanchet, J.-P. and Lazare, M. 1992. The Canadian Climate Centre second generation general circulation model and its equilibrium climate. *J Climate* **5**, 1013–1044.

Mo, R., Fyfe, J. and Derome, J. 1998. Phase-locked and asymmetric correlations of the wintertime atmospheric patterns with the ENSO. *Atmos-Ocean* **36**, 213–239.

Namias, J., Yuan, X. and Cayan, D. R. 1988. Persistence of north pacific sea surface temperature and atmospheric flow patterns. *J. Climate* **1**, 682–703.

Opsteegh, J. D. and Van den dool, H. M. 1980. Seasonal differences in the stationary response of a linearized primitive equation model: Prospects for long range weather forecasting? *J. Atmos. Sci*. **37**, 2169–2185.

Parker, D. E., Folland, C. K., Bevan, A., Ward, M. N., Jackson, M. and Maskell, K. 1995. Marine surface data for analyses of climatic fluctutations on interannual and century time scales. In: *Natural Climate Variability on Decade to Century Timescales*, (eds. D. G. Martinson, K. Bryan, M. Ghil, M. M. Hall, T. R. Karl, E. S. Sarachik, S. Sorooshian and L. D. Talley), U.S. Natl. Acad. Sci., Washington, DC, 241–250.

Peng, S., Robinson, W. A. and Hoerling, M. P. 1997. The modeled atmospheric response to midlatitude SST anomalies and its dependence on background circulation states. *J. Climate* **10**, 971–987.

Peng, P., Kumar, A., Barnston, A. G. and Goddard, L. 2000. Simulation skills of the SST-forced global climate variability of the NCEP-MRF9 and the SCRIPPS-MPI ECHAM3 models. *J. Climate* **13**, 3657-3679.

Renwick, J. A. and Wallace, J. M. 1996. Relationship between North Pacific wintertime blocking, El Niño, and the PNA pattern. *Mon. Wea. Rev*. **124**, 2071–2076.

Reynolds, R. W. and Smith, T. M. 1994. Improved global sea surface temperature analysis using optimum interpolation. *J. Climate* **7**, 929–948.

Rice, J. A. 1995. *Mathematical statistics and data analysis, second edition*. Duxbury Press, Belmont, CA, 602 pp.

Ropelewski, C. F. and Halpert, M. S. 1986. North American temperature and precipitation patterns associated with the El Niño/Southern Oscillation. *Mon. Wea. Rev*. **114**, 2352–2362.

Rowell, D. P 1998. Assessing potential seasonal predictability with an ensemble of multidecadal GCM simulations. *J. Climate* **11**, 109–120.

Saravanan, R. 1998. Atmospheric low-frequency variability and its relationship to midlatitude SST variability: Studies using the NCAR Climate System Model. *J. Climate* **11**, 1386–1404.

Scheffe, H. 1959. *The analysis of variance*. John Wiley and Sons, New York, 479 pp.

Searle, S. R., Casella, G. and McCulloch, C. E. 1992. *Variance components*. John Wiley and Sons, New York, 501 pp.

Shabbar, A. and Khandekar, M. 1996. The impact of El Niño-Southern Oscillation on the temperature field over Canada. *Atmos-Ocean*. **34**, 401–416.

Sheng, J. 1999. Correlation between the Pacific/North American pattern and the eastward propogation of sea surface temperature anomalies in the North Pacific. *J. Geophys. Res*. **104**, 30 885–30 895.

Simmons, A. J., Wallace, J. M. and Branstrator, G. W. 1983. Barotropic wave propogation and instability, and atmospheric teleconnection patterns, *J. Atmos. Sci*. **40**, 1363–1392.

Straus, D. M. and Shukla, J. 2000. Distinguishing between the SST-forced variability and internal-variability in mid latitudes: Analysis of observations and GCM simulations. *Q. J. R. Meteorol. Soc*. **126**, 2323–2350.

Wallace, J. M. and Gultzler, D. S. 1981. Teleconnections in the geopotential heights field during the northern hemisphere winter. *Mon. Wea. Rev*. **109**, 784–812.

Wang, H. and Fu, R. 2000. Winter monthly mean atmospheric anomalies over the North Pacific and North America associated with El Niño SSTs. *J. Climate* **13**, 3435–3447.

Wang, X. L. and Zwiers, F. W. 1999. Interannual variability of precipitation in an ensemble of AMIP climate simulations conducted with the CCC GCM2. *J. Climate* **12**, 1322–1335.

Zwiers, F. W. 1996. Interannual variability and predictability in an ensemble of AMIP climate simulations conducted with the CCC GCM2. *Clim. Dynam*. **12**, 825–847.

Zwiers, F. W., Wang, X. L. and Sheng, J. 2000. Effects of specifying bottom boundary conditions in an ensemble of atmospheric GCM simulations. *J. Geophys. Res*. **105**, 7295–7315.